ELSEVIER

Journal of Molecular Liquids 96–97 (2002) 195–206

journal of MOLECULAR LIQUIDS

www.elsevier.com/locate/molliq

Water in nanopores in equilibrium with a bulk reservoir - Gibbs ensemble Monte Carlo simulations

Ivan Brovchenko and Alfons Geiger*

Physikalische Chemie, Universität Dortmund, 44221 Dortmund, Germany

Water confined in cylindrical and spherical nanopores in equilibrium with a bulk reservoir at atmospheric pressure was simulated in the Gibbs ensemble. Capillary condensation or capillary evaporation is observed depending on the strength of the water-pore interaction. Liquid water exists in the pore by forming two prominent orientationally ordered layers near the pore wall, whereas the properties of the rest of the water are close to the bulk. Water oxygens in the outermost layer show ordering in hydrogen-bonded quasi-planar polygons, which improves with strengthening water-pore interaction, decreasing temperature and decreasing pore size.

1. INTRODUCTION

The structural and dynamical properties of a fluid, which is confined in a nanopore, differ significantly from the bulk due to the geometrical confinement and the interaction with the pore wall. The investigation of the fluid properties in nanopores first of all requires the knowledge of its phase state. In addition to the usual liquid-vapour phase transition, surface phase transitions (such as layering transitions) may occur in the pores [1].

Two typical thermodynamical situations may be distinguished: "closed" and "open" pores. In a "closed" pore the average fluid density in the pore is fixed at some arbitrarily chosen value (in experiments this corresponds to different degrees of pore filling by the fluid). One-phase states or two-phase coexistence may be expected, depending on the average fluid density in the pore, temperature and pore parameters. First simulations of water phase diagrams in nanopores show two-phase coexistence in a wide range of density and in a temperature interval, which essentially extends above room temperature [2]. In hydrophilic pores one or two layering transitions appear in addition to the liquid-vapour transition.

In the "open" pore the density and phase state of the fluid is determined by the thermodynamic equilibrium with an external bulk reservoir. The most important practical situation corresponds to the equilibrium with a bulk fluid at ambient pressure. Either liquid (by capillary condensation) or vapour (by capillary evaporation) states of the fluid in the pore are expected [3], depending on the pore parameters and temperature. The determination of the pore parameters which separate these two regimes is a necessary preliminary condition for the correct analysis of the structural properties of the fluid in the pore. The phase behaviour

* Author to whom correspondence should be addressed

0167-7322/02/$ - see front matter © 2002 Elsevier Science B.V. All rights reserved.
PII S0167-7322(01) 00003-X

and structural properties of water in "open" cylindrical and spherical nanopres in equilibrium with a bulk reservoir at atmospheric pressure is considered in the present paper.

Numerous molecular dynamics and Monte Carlo (MC) simulations of liquid water in nanopores were reported (see, for example [4-18]). Various ways to establish an equilibrium with a bulk were used (see [17] for more detailed analysis). In most of the simulations the liquid water density in the pore (average density or density in the pore center) was fixed at approximately the bulk density [4-10]. However, such an adjustment of the water density to the bulk value does not mean that the confined water is in equilibrium with the bulk. Such an approach assumes that the liquid in the center of the pore is not influenced by the confinement or by interactions with the surface. This may be correct for large slit-like pores, but it is obviously not appropriate for nanopores and especially pores with cylindrical or spherical geometry.

Using experimentally measured water densities in pores for the computer simulation [11,12] also does not guarantee meaningful results, due to the unavoidable differences between real and model systems and due to the uncertainties in the determination of the simulated and experimental pore volumes.

A natural way to obtain equilibrium with a bulk reservoir is the use of MC simulations in the grand canonical ensemble with the bulk value of the chemical potential. This approach was widely used for the simulation of simple model liquids in pores of different types, whereas there are only a few applications for water (see, for example [13-15]). The quality of the chemical equilibration between pore and bulk in a grand canonical MC simulation depends both on the accuracy of the computation of the chemical potential of the bulk water and on the equilibration of the pore water.

A Gibbs ensemble simulation provides the most direct and accurate way for the equilibration of a confined and a bulk liquid by an essential number of molecular transfers between the two phases [19]. As mechanical equilibrium has not to be established explicitly in such systems, the bulk water may be kept at constant pressure and temperature, and simultaneously the pore water at the same temperature and constant pore volume. There is a close resemblance to a grand canonical ensemble simulation, but instead of specifying a common value of the chemical potential for both systems, the simulation box with the bulk water is used for chemical equilibration directly. This procedure yields a higher accuracy of the simulation by speeding up the equilibration process. The bulk water may be kept in the vapour phase [16], but as available water models were fitted mainly to the properties of condensed water, using the liquid as bulk phase seems to me more appropriate. This determined our choice to use the Gibbs ensemble for the simulation of water in pores in equilibrium with bulk liquid water.

Experimental studies of water confined in pores show the existence of two distinguishable species: "free" water in the center of the pore and "bound" water near the pore surface [20-25]. The shift of the freezing temperature of the "free" water is roughly inversely proportional to the pore radius, whereas for the "bound" water the phase transition is smeared out and its temperature range does not depend on the pore size. Estimates of the thickness of the "bound" water layer by different experimental methods yield 1 to 3 water monolayers [20-25]. X-ray diffraction experiments show that the "bound" water possesses little short-range order [24].

Computer simulations of water in pores show various degrees of water layering near the pore surface: from a strong layering with a few distinct layers near strong-interacting surfaces to a weak layering without essential variations of the density near weak-interacting or free

surfaces. Without specific water-pore interactions the water molecules show orientational ordering near the surface with a tendency to keep the orientation of the dipole moment parallel to the surface in order to maximize the number of water-water hydrogen bonds. The degree of water layering near the surface and its orientational ordering depend on the pore parameters, but also on the choice of the average water density in the pore. The more or less arbitrary choices of the number of water molecules in the pores in most of the reported simulations complicate a systematic analysis of the water properties in the pore.

In the present paper, based on simulations of water in pores in equilibrium with bulk water, we analyse the dependence of the water properties on water-pore interaction, pore size and temperature.

2. SIMULATION METHOD

512 TIP4P [26] water molecules in a cubic box with periodic boundary conditions were used to reproduce bulk water at P = 1 bar. Intermolecular interactions were calculated up to a cutoff distance of 12 A and long-range corrections were included for the Lennard-Jones potentials only. Cylindrical and spherical pores with radii R_C from 6 to 20 A were considered. The length of the cylindrical pore was fixed at $2R_C$. The water-water interactions in the pore were calculated without cutoff. The water-pore interaction was simulated as Lennard-Jones (9-3) potential

$$U_{w\text{-}p}(r) = \varepsilon[(\sigma/r)^9 - (\sigma/r)^3] ,$$

where r is the distance between the water oxygen and the pore wall along the radius vector. The parameter σ in this potential was fixed to 2.5 A, the parameter ε varied to change the well-depth $U = -0.385\varepsilon$ from -0.46 to -5.77 kcal/mol. This range of strength of the water-substrate interaction approximately corresponds to a variation of the substrate from hydrocarbon-like to metallic.

Initial configurations were produced by equilibration in the NPT ensemble for bulk water and in the NVT ensemble for water in pores with various numbers of molecules.

2.1 Gibbs ensemble simulation

The equilibration between the pore water and the bulk liquid water was provided by MC simulations in the Gibbs ensemble. In order to achieve equilibrium an essential number of molecular transfers between the two systems must be provided. Low efficiency of molecular transfers is the main problem in Gibbs ensemble simulations. This problem grows strongly for associated liquids as water and especially for the coexistence of two dense phases. The efficiency of the molecular transfer attempts in the MC runs was improved by a biased choice of more loosely bound molecules for the deletion [2,17] and by applying a sequence of interatomic distance criteria to avoid unsuccessful attempts of insertion. In both cases the acceptance probability has to be corrected by a factor, which was obtained from the probability distributions of energy and shortest interatomic distances, respectively. Simulations in the Gibbs ensemble were done at T = 300 K and T = 350 K. When decreasing the temperature to T = 250 K, equilibrium was achieved only for small and weakly attractive pores.

2.2 Calculation of the structural properties of water in pores

The average water densities in the pores, obtained by the Gibbs ensemble simulation, were used for the subsequent MC simulations in the canonical NVT ensemble. In order to study the influence of decreasing temperature, some pores were simulated at T = 200 K, keeping the water density in the pore equal to the one obtained by equilibration at T = 300 K. Structural analysis was performed every 1000 MC steps during runs of at least $2*10^5$ configurations.

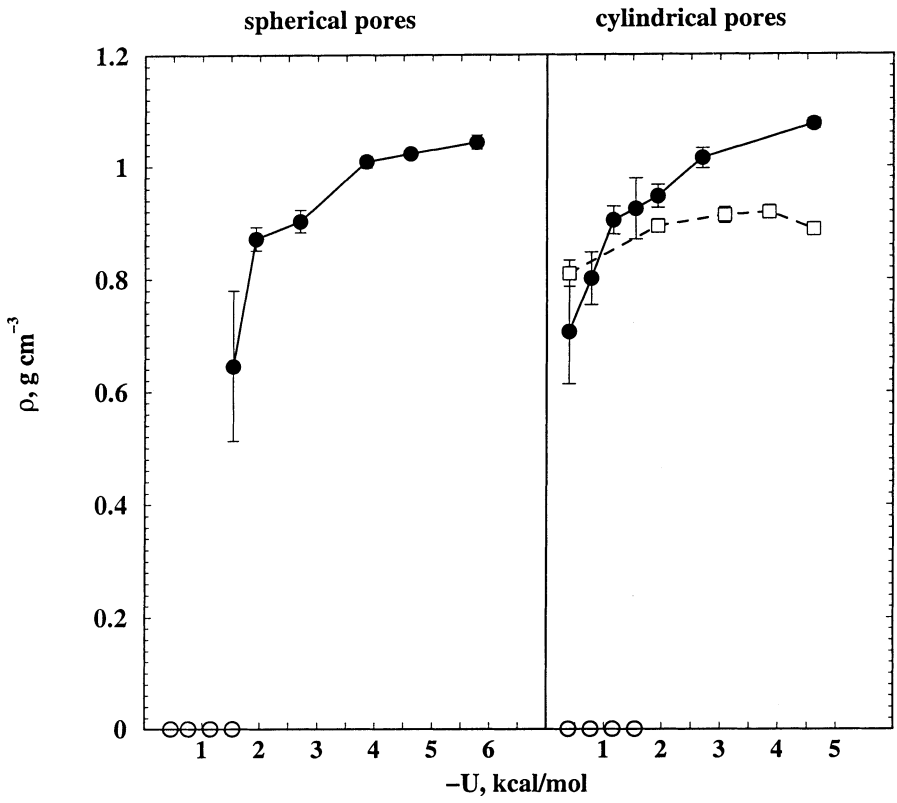

Fig.1. Dependence of the average water density in spherical and cylindrical pores on the water-pore potential well-depth U (open circles: adsorption, close circles: desorption). R_C = 12 A. T = 300 K. Open squares show the water density at the liquid branches of the coexistence curves for closed cylindrical pores [2]. Lines are guides for the eyes only.

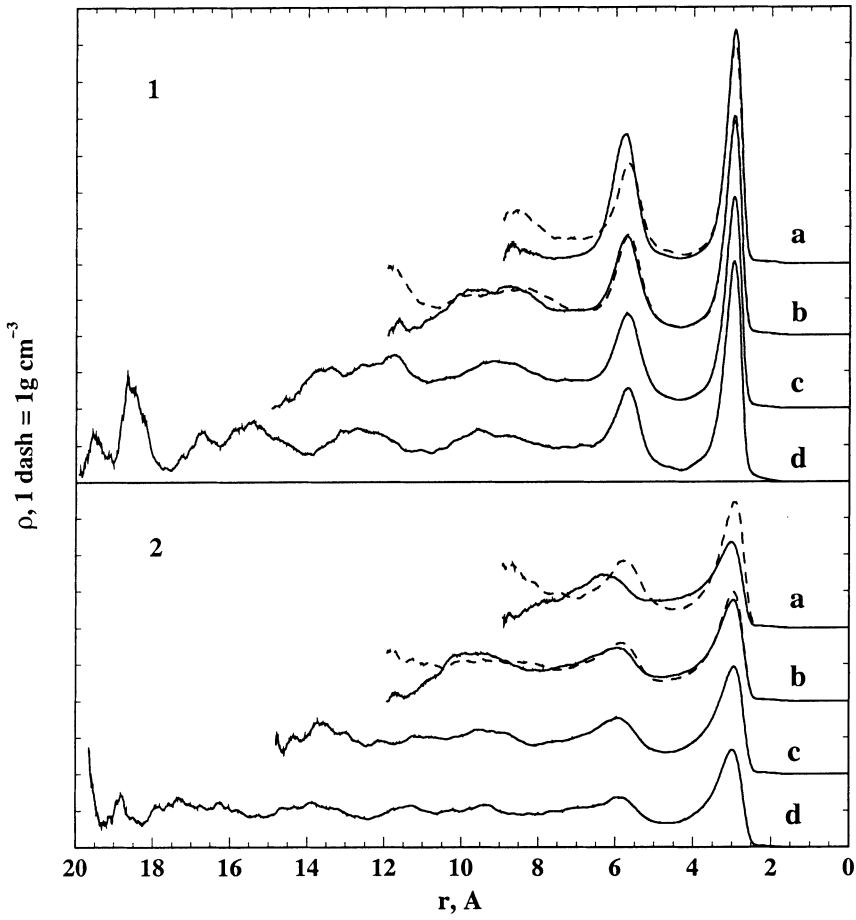

Fig.2. Water density along the pore radius. 1. U = -4.62 kcal/mol. 2. U = -1.93 kcal/mol. a) R_C = 9 A; b) R_C = 12 A; c) R_C = 15 A; d) R_C = 20 A. T = 300 K. Solid lines: spherical pores; dashed lines: cylindrical pores.

pore wall reflects an orientation of the OH vectors towards the first layer. Such orientational ordering in the first two layers is almost identical in spherical and cylindrical pores. Strengthening water-pore interaction improves this ordering strongly. The temperature effect is not so pronounced (Fig.3), whereas a change of the pore wall curvature when the pore

The local water density was calculated based on the positions of the O and H atoms. The analysis of the structural properties of the pore water was done separately for the different water layers, which were distinguished by the density variation along the pore radius.

When calculating the pair correlation functions of water in spherical pores, the excluded volume effect was taken into account by numerical integration of the volumes of the considered spherical shells, accessible to oxygen atoms. Two types of correlations were considered: correlations between the oxygens in a specific layer and all other molecules and correlations between the oxygens of the considered layer only. In the latter case "in-plane" pair correlation functions were calculated for cylindrical pores.

3. RESULTS

The increase of the average water density in the pore with strengthening water-pore interaction is presented in Fig.1. The values of the water density were obtained by assuming that the water occupies the pore up to a distance $\sigma/2$ from the pore wall, where σ = 2.5 A (from the water-pore potential). The presented results show, that both capillary condensation and capillary evaporation may take place in the considered pores depending on the water-pore interaction. Note that in the case of the capillary condensation the change of the water density in the pore with strengthening pore-water interaction amounts up to 20 %.

The obtained densities depend on the initial state of the system in some range of the parameter U due to a trapping of the system in metastable states. For spherical pores (Fig.1, left panel) this hysteresis interval is small and the critical value U_C, which separates capillary evaporation and capillary condensation, may be estimated to U_C = -1.5 kcal/mol.

The hysteresis interval is substantially larger for the cylindrical pores (Fig.1, right panel). In order to localize the position of the equilibrium liquid-vapour transition, we use the results of the previous Gibbs ensemble simulations of the liquid-vapour coexistence curves in closed cylindrical pores [2]. The densities at the liquid branch of the coexistence curves are shown by squares in Fig.1. The intersection of the two dependences, presented in Fig.1 for cylindrical pores, corresponds to the equilibrium liquid-vapour transition and the critical value U_C may be estimated as U_C = -1.0 kcal/mol.

NVT MC simulations at the water densities, obtained by the Gibbs ensemble simulations, were used to obtain the structural properties of water in the pores with U = -4.62 kcal/mol and -1.93 kcal/mol. The water density profiles along the pore axis are presented in Fig.2. Two prominent water layers near the pore wall are observed in all cases (the fluctuations of the density in the region close to the center of the pore reflect only decreasing statistical accuracy when the volume of the spherical or cylindrical shells goes to zero).

The two water layers near the pore wall possess a strong orientational ordering, which is absent in the inner water. The ordering may be clearly seen from the analysis of the hydrogen and oxygen density profiles along the pore radius (Fig.3). The hydrogen density maxima at 2 A and 4 A from the pore wall (in 1 A distance from the principle maximum of the oxygen distribution at 3 A) reflect the preferential orientations of the OH vectors outwards and inwards along the pore radius, the coincidence of the main peaks of the oxygen and hydrogen distributions at 3 A indicates that most of the OH vectors are oriented normally to the pore radius. In the second water layer the maximum of the hydrogen density around 5 A from the

radius increases from 6 to 15 A [18] effects the orientational ordering noticeably (more OH vectors become oriented towards the pore center), a subsequent increase of the pore radius to 20 A has only little effect (Fig.3).

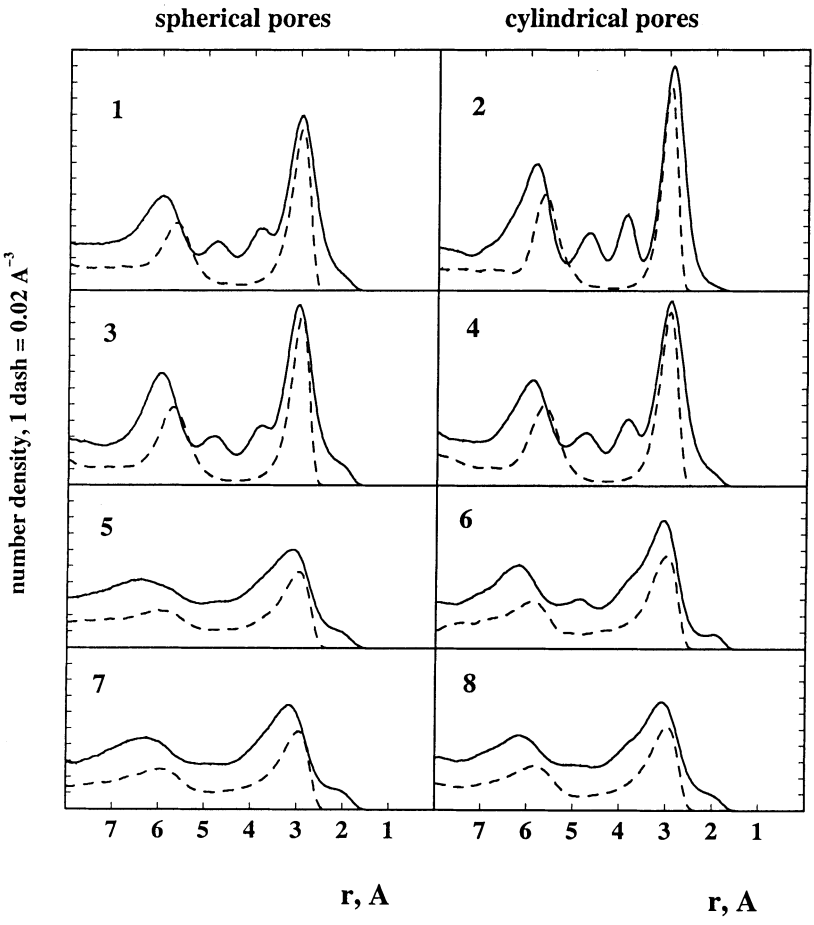

Fig.3. Oxygen atom (dashed line) and hydrogen atom (solid line) density profiles along the pore radius. 1 – 4: U = -4.62 kcal/mol; 5 – 8: U = -1.93 kcal/mol. T = 300 K excluding 2 and 6, where T = 200 K. R_C = 12 A (2 - 4, 6 – 8) and R_C = 20 A (1,5)

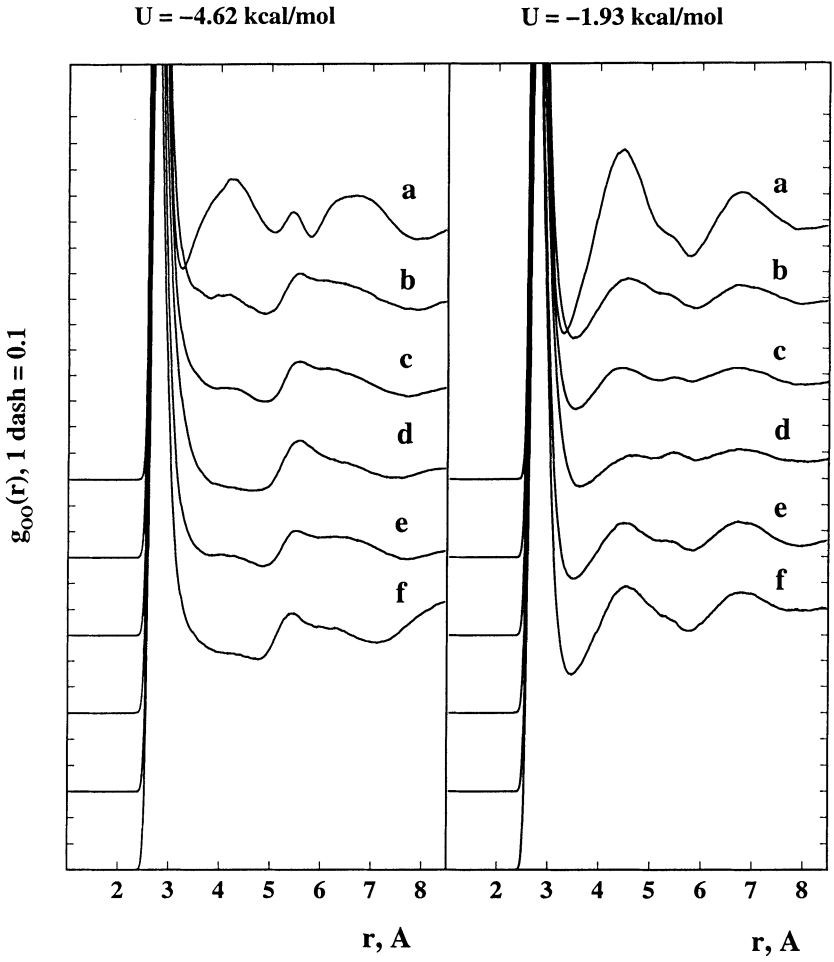

Fig.4. Radial distribution functions $g_{OO}(r)$ of water in the first layer in spherical pores (correlations with all other molecules are included): a) R_C = 20 A, T = 200 K; b) R_C = 20 A, T = 300 K; c) R_C = 15 A, T = 300 K; d) R_C = 12 A, T = 350 K; e) R_C = 12 A, T = 300 K; f) R_C = 9 A, T = 300 K.

To calculate the pair correlation functions, the water in the pore was subdivided into three regions, based on the location of the density minima: first water layer, second water layer and inner water (Fig.2). In all considered pores the $g_{OO}(r)$ for the inner water and the water in the second water layer are qualitatively similar to the $g_{OO}(r)$ for the bulk water [17], whereas the $g_{OO}(r)$ in the first water layer shows an additional maximum around 5.45 A (Fig.4 and 5). This

maximum increases with strengthening water-pore interaction but is not very sensitive to the variation of temperature. A decreasing temperature causes an increase of the maxima around 4.5 A and 6.7 A, which reflect the local tetrahedral structure of water.

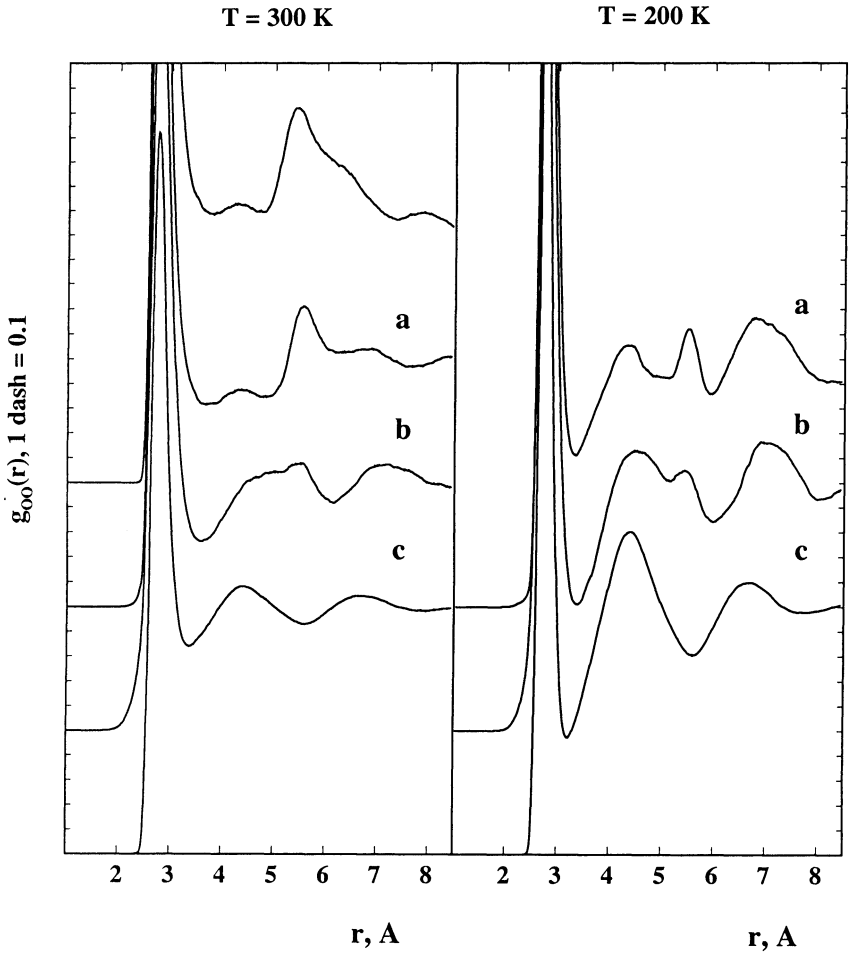

Fig.5. "In-plane" pair correlation functions $g_{OO}(r)$ of water in the first layer of the cylindrical pores. R_C = 9 A. a) U = -4.62 kcal/mol; b) U = -1.93 kcal/mol, c) bulk water. Upper curve in the left panel: $g_{OO}(r)$ of water in a spherical pore with R_C = 9 A and U = -4.62 kcal/mol, which includes correlation between molecules in first layer only.

The arrangement of the water oxygens and the hydrogen bonds in the first water layer is illustrated in Fig.6. Hydrogen-bonded water polygons of different size are observed. The number of such polygons increases with strengthening water-pore interaction, decreasing temperature and decreasing pore size [18]. Specific arrangements of the oxygens in more or less straight lines give rise to the appearance of the maximum of $g_{OO}(r)$ at 5.45 A, which approximately corresponds to a doubling of the first maximum position.

4. DISCUSSION

The presented simulation of confined water in equilibrium with a bulk reservoir reveals the existence of a threshold value for the water-pore interaction, which separates capillary evaporation from capillary condensation. This agrees with experimental investigations of water adsorption in pores with different ratios of hydrophilic and hydrophobic groups: liquid water stops penetrating the pore strictly at some level of hydrophobicity [26]. Strengthening of the water-pore interaction causes a marked increase of the density of liquid water in the pore (up to 20% in the considered range of interaction).

In the case of the strongly hydrophobic pores the bulk water at atmospheric pressure coexists with a vapour phase in the pore (see Fig.1). A simulation of liquid water in such pores is valid only when a higher pressure of the bulk water is assumed. The substantial change of the liquid water density in the hydrophilic pores with strengthening water-pore interaction emphasizes the importance of a correct equilibration with the bulk, especially in view of the fact that the water properties strongly depend on its density. A less accurate determination of the liquid water density means that it is in equilibrium with bulk water, which is kept at an unknown pressure. A strong underestimation of the liquid water density in the pore (below the dashed line, shown in Fig.1 for cylindrical pores) causes serious problems, as it means entering a two-phase region and simulating a thermodynamically unstable state.

The most important structural feature of confined liquid water is the appearance of two prominent layers near the pore wall. These two layers always accompany the existence of liquid water both in cylindrical and spherical pores. There are no essential changes of the water density profiles near the pore wall in a wide temperature range (especially in hydrophilic pores). The existence of two stable orientationally ordered water layers agrees with experimental observation of "bound" water near the pore wall with thickness of 1 to 3 monolayers [20-25].

Water in the first layer shows a high orientational ordering and arrangements in quasi-planar hydrogen-bonded polygons (Fig.6), that results in the appearance of an additional maximum of the oxygen-oxygen pair correlation function at 5.45 A (Fig.4 and 5). In contrast to the maximum at 5.45 A the local tetrahedral water structure in the first layer, represented by the two peaks at 4.5 A and 6.7 A, is very sensitive to changes of the temperature. This agrees with experimental studies of the distortion of the tetrahedral water structure in cylindrical pores at different temperatures [28]. Water in the second layer shows a specific orientational ordering, by this providing a connection between the distorted first layer and the tetrahedrally ordered inner water. There is no additional oxygen-oxygen peak at 5.45 A in the second layer.

The structural properties of the inner water in general are close to the properties of bulk water. Some differences were found in the radial distribution functions of the centers of the

non-short-circuited hydrogen-bonded hexagons [18]. These differences indicate a trend of the structure of the inner water towards the structure of cubic ice.

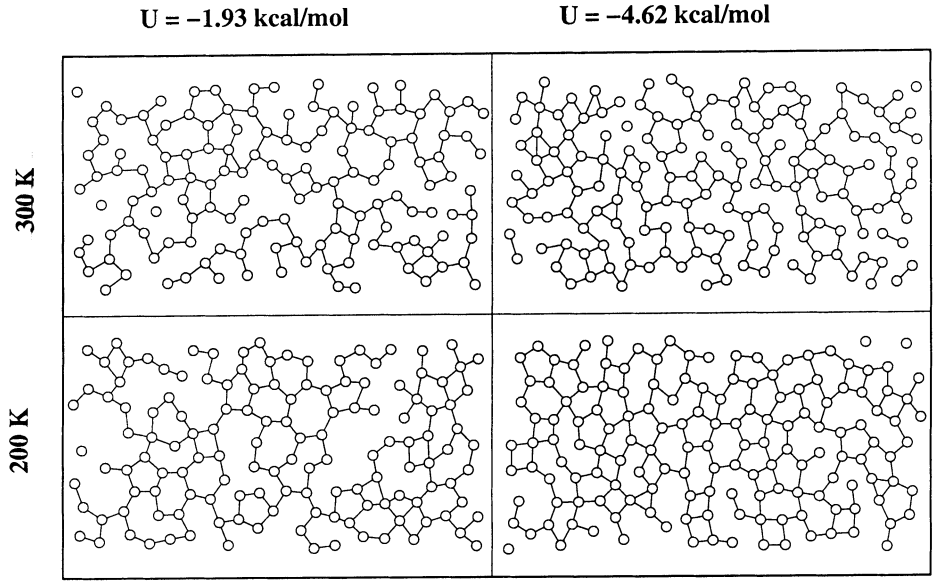

Fig.6. Arrangement of the oxygen atoms in the first water layer of the cylindrical pores with R_C = 12 A. Hydrogen bonds are shown by lines.

REFERENCES

1. R.Evans, J.Phys.: Condens.Matter., 2 (1990) 8989.
2. I.Brovchenko, A.Geiger and A.Oleinikova, Phys.Chem.Chem.Phys., 3, (2001).
3. P.B.Balbuena and K.E.Gubbins, Langmuir, 9 (1993) 1801.
4. S.H.Lee and P.J.Rossky, J.Chem.Phys., 100 (1994) 3334.
5. L.Zhang, H.T.Davis, D.M.Kroll and H.S.White, J.Phys.Chem., 99 (1995) 2878.
6. C.Harting, W.Witschel and E.Spohr, J.Phys.Chem.B, 102 (1998) 1241.
7. E.Spohr, J.Chem.Phys., 106 (1997) 388.
8. E.Spohr, C.Harting, P.Gallo and M.Rovere, J.Mol.Liquids, 80 (1999) 165.
9. T.W.Allen, S.Kuyucak and S.-H. Chung, J.Chem.Phys., 111 (1999) 7985.
10. J.Faeder and B.M.Ladanyi, J.Phys.Chem.B, 104 (2000) 1033.

11. M.Rovere, M.A.Ricci, D.Velatti and F.Bruni, J.Chem.Phys., 108 (1998) 9859.
12. P.Gallo, M.Rovere, E.Spohr, Phys.Rev.Lett., 85 (2000) 4317.
13. J.C.Shelley, G.N.Pattey, D.R.Berard, and G.M.Torrie, J.Chem.Phys., 107, (1997) 2122.
14. L.D.Gelb, K.E.Gubbins, R.Radhakrishnan, and M.Sliwinska-Bartkowiak, Rep.Prog.Phys., 62 (1999) 1573.
15. A.Delville, J.Phys.Chem., 97 (1993) 9703.
16. S.C.McGrother and K.E.Gubbins, Mol.Phys., 97 (1999) 955.
17. I.Brovchenko, D.Paschek and A.Geiger, J.Chem.Phys., 113 (2000) 5026.
18. I.Brovchenko, A.Geiger, D.Paschek Fluid Phase Equilibria, (2001), accepted.
19. A.Z.Panagiotopoulos, Mol.Phys., 62 (1987) 701.
20. D.C.Steytler, J.C.Dore and C.J.Wright, Mol.Phys., 48 (1983) 1031.
21. K.Overloop and L. Van Gerven, J.Magn.Res., A101 (1993) 179.
22. E.W.Hansen, M.Stocker and R.Schmidt, J.Phys.Chem., 100 (1996) 2195.
23. E.W.Hansen, E.Tangstad and E.Myrvold, J.Phys.Chem., B101 (1997) 10709.
24. K.Morishige and K.Nobuoka, J.Chem.Phys., 107 (1997) 6965.
25. K.Morishige and K.Kawano, J.Chem.Phys., 110 (1999) 4867.
26. W.L.Jorgensen, J.Chandrasekhar and J.D.Madura, J.Chem.Phys., 79 (1983) 926.
27. Y.Hirama, T.Takahashi, M.Nino and T.Sato, J.Colloid Interface Sci., 184 (1996) 349.
28. P.Smirnov, T.Yamaguchi, S.Kittaka, S.Takahara and Y.Kuroda, J.Phys.Chem., B104 (2000) 5498.

ACKNOWLEDGEMENTS

This work was supported by Ministerium für Schule und Weiterbildung, Wissenschaft und Forschung des Landes Nordrhein-Westfalen.